Scilight

Nonlinear Analysis and Computer Simulations

https://www.sciltp.com/journals/nacs

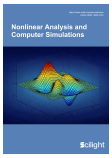

Article

Equal Tangent Length Partitioning for High-Precision Numerical Integration

Jing Shi [1,*], Wanqing Song [2] and Mingcan Sun [3]

[1] School of Information Engineering, Minnan University of Science and Technology, Quanzhou 362700, China
[2] School of Electronic and Electrical Engineering, Minnan University of Science and Technology, Quanzhou 362700, China
[3] School of Information Engineering, Minnan University of Science and Technology, Quanzhou 362700, China
* Correspondence: shijing0103@126.com; Tel.: +86-138-6078-8853

How To Cite: Shi, J.; Song, W.; Sun, M. Equal Tangent Length Partitioning for High-Precision Numerical Integration. *Nonlinear Analysis and Computer Simulations* **2026**, *1*(2), 6. https://doi.org/10.53941/nacs.2026.100006

Received: 18 November 2025
Revised: 15 January 2026
Accepted: 17 March 2026
Published: 2 April 2026

Abstract: In this study we develop a novel approach for improvement of the precision of numerical integration by using equal tangent slopes in order to partition the integration interval. As a result, two new composite numerical integration formulas are derived. Using continuous function properties, it is possible to analyze the error and convergence of these formulas. A practical example confirms the effectiveness of this method in improving the accuracy of numerical integration. Additionally, the paper delves into the convergence properties and the error reduction capabilities of the new formulas compared to the traditional trapezoidal and Simpson's rules. The limitations of the developed approach are briefly discussed.

Keywords: numerical integration; equal tangent length; convergence

2020 MSC: 65D30

1. Introduction

Numerical integration is a cornerstone of applied mathematics, engineering, and computational sciences, providing an essential tool for approximating definite integrals when analytical solutions are not feasible. Classical methods, such as the Trapezoidal Rule and Simpson's Rule, have long been favored for their simplicity and effectiveness across a wide variety of functions. However, as the complexity of problems in modern research increases, these traditional methods often struggle to meet the demands for higher accuracy and efficiency, motivating the development of more advanced numerical integration techniques.

Recent literature has made significant strides in addressing these challenges through innovative approaches. For instance, in [1], a comparative convergence analysis was performed for integrating rational, weakly singular, and trigonometric test functions over an ellipsoid, utilizing both Gaussian and generalized Gaussian quadrature rules. The study introduced novel transformations to enable numerical integration over curved tetrahedral elements, enhancing performance across all test cases. Similarly, in [2], an expression for the periodic first derivative of Green's function in real space was proposed, offering an alternative method to compute the periodic Green's operator by periodically summing the free-space Green's operator with an appropriate quadrature rule.

Numerical integration has also been adapted to probabilistic and nonlinear frameworks. In [3], the Bayes–Sard quadrature method was explored within the context of sigma-point filters, formalizing quadrature error uncertainty within a probabilistic model. A key contribution of this work was deriving classical quadratures as special cases of the Bayes–Sard method, providing a unified framework for quadrature techniques. In [4], a numerical method for the Schrödinger map (SM) was developed using the Hasimoto transform, which connects the SM flow to the cubic nonlinear Schrödinger (NLS) equation. Leveraging this transform, the authors constructed

fully explicit and unconditionally stable symmetric integrators for the SM equation, demonstrating the versatility of numerical integration in tackling complex differential equations.

Efforts to enhance classical methods have also yielded notable advancements. In [5], new integration formulas of arbitrary accuracy order were proposed based on B-spline relations from Amat et al. Defined as perturbations of the Trapezoidal Rule, these formulas were proven to achieve higher-order approximations and were extended to multiple dimensions. Meanwhile, the authors of study [6], introduced an improved numerical integration method aimed at predicting the stability of milling operations. Application of the Lagrange-Simpson interpolation scheme represented a noteworthy contribution to advancements in manufacturing technologies, illustrating the broad impact of numerical integration on industrial applications. Additionally, in [7], the authors engaged in an in-depth study of the Trapezoidal and Simpson's rules for numerical integration, offering a new perspective through which the efficiency and accuracy of these traditional methods were analyzed. Their insights provided valuable contributions to the knowledge base regarding the application of numerical integration to integral problems.

The applicability of numerical integration extends to practical domains such as environmental engineering and energy management. In [8], the role of numerical integration in modeling reverse osmosis systems was highlighted, emphasizing its importance in optimizing processes critical for water quality maintenance. In [9], an algorithm based on the Trapezoidal Rule was developed to improve the efficiency of photovoltaic power generation under both uniform and partially shaded conditions, showcasing the adaptability of numerical methods in energy optimization. Furthermore, ref. [10] investigated the integration of the Taylor series with the Trapezoidal Rule, bridging discrete and continuous analysis and providing a robust tool for evaluating dynamic systems.

In summary, these studies highlighted not only the robustness of numerical integration methods, but also their applicability in environmental engineering, energy optimizations etc. These studies underscore the importance of numerical integration in modern research.

In this work we elaborate two new composite numerical integration formulas and use identical tangent slopes to split integration intervals based on the previously discussed references. Our computational example demonstrates the applicability of the method for numerical integration, and modest errors, strong convergence and ease of implementation underscore our contribution.

2. Preliminaries

In this section, we introduce numerical integration and classical numerical integration methods, and lay the groundwork for the equal tangent length partitioning approach.

2.1. Numerical Integration

The curvilinear trapezoid is formed by the curve $y = f(x)$, the line $x = a$,the line $x = b$ and the x-axis, where the curve is defined on $[a,b]$. If $f(x)$ is a continuous function on $[a,b]$, then the area of the curvilinear trapezoid is

$$I(f) = \int_a^b f(x)dx$$

Definition 1 [11]**.** *With a set of nodes*

$$a \le x_0 < x_1 < x_2 < \cdots < x_n \le b,$$

we determine the values of $f(x_k)$ $(k = 0,1,\cdots,n)$. *The one can construct the Lagrange interpolation polynomial of degree* n *:*

$$L_n(x) = \sum_{k=0}^{n} l_k(x) f(x_k).$$

It is easy to obtain the antiderivative of the algebraic polynomial $f(x)$. *Then we have:*

$$I_n(f) = \int_a^b L_n(x)dx = \sum_{k=0}^{n} \int_a^b l_k(x)dx\, f(x_k) = \sum_{k=0}^{n} C_k f(x_k).$$

as the approximate value of $I(f)$. *The quadrature formula*

$$I_n(f)=\sum_{k=0}^{n}C_k f(x_k).$$

is called an interpolation quadrature formula, where the quadrature coefficient is

$$C_k=\int_a^b l_k(x)dx,\ k=0,1,\cdots,n \tag{1}$$

and $l_k(x)\ (k=0,1,\cdots,n)$ *is the Lagrange interpolation basis function.*

2.2. Classical Numerical Integration Methods

Two widely used composite numerical integration methods are the Trapezoidal Rule and Simpson's Rule, which rely on equally spaced partitions. According to Definition 1, we obtain the following Newton-Cotes formula with the degree n.

Definition 2 [11]**.** *Assume that the interval* $[a,b]$ *is divided into* n *equal parts with the step size of* $h=\dfrac{b-a}{n}$ *and equidistant nodes* $x_k=a+kh\ (k=0,1,\cdots,n)$*, then*

$$I_n(f)=(b-a)\sum_{k=0}^{n}C_k^{(n)}f(x_k) \tag{2}$$

is called Newton-Cotes formula of degree n*, where* $C_k^{(n)}$ *is called the Cotes coefficient. Substitution of* $x_k=a+th$ *into (1) gives*

$$C_k^{(n)}=\frac{h}{b-a}\int_0^n\prod_{\substack{j=0\\ j\neq k}}^{n}\frac{t-j}{k-j}dt=\frac{(-1)^{n-k}}{nk!(n-k)!}\int_0^n\prod_{\substack{j=0\\ j\neq k}}^{n}(t-j)dt.$$

Let $n=1$, then substituition of $C_0^{(1)}=C_1^{(1)}=\dfrac{1}{2}$ into expression (2) gives us the trapezoidal integration rule

$$T=I_1(f)=\frac{b-a}{2}[f(a)+f(b)] \tag{3}$$

If $n=2$, then Cotes coefficients are the following

$$C_0^{(2)}=\frac{1}{4}\int_0^2(t-1)(t-2)dt=\frac{1}{6},$$

$$C_1^{(2)}=-\frac{1}{2}\int_0^2 t(t-2)dt=\frac{4}{6},$$

$$C_2^{(2)}=\frac{1}{4}\int_0^2 t(t-1)dt=\frac{1}{6}.$$

Substitution of the Cotes coefficients in formula (2) gives us the Simpson integration rule

$$S=I_2(f)=\frac{b-a}{6}[f(a)+4f(\frac{a+b}{2})+f(b)]. \tag{4}$$

The error of the Simpson's Rule is given by

$$E_{simp}=-\frac{b-a}{180}f^{(4)}(\xi)(\frac{b-a}{2})^4,\ \xi\in[a,b].$$

Due to the instability of the Newton-Cotes formula as the order increases, enhancing the degree of precision for numerical integration simply through incrementing the order is not viable. Given that definite integrals have additive properties over subintervals, an integral can be evaluated by partitioning the interval into several subintervals, applying the rule independently on each, and subsequently aggregating the results. This technique is referred to as composite numerical integration.

Definition 3 *Assume that the interval* $[a,b]$ *is divided into* n *equal parts with the step size* $h=\frac{b-a}{n}$ *and equidistant nodes* $x_k=a+kh$, $k=0,1,\cdots,n$, *then*

(a) On each subinterval $[x_k,x_{k+1}]$ $(k=0,1,\cdots,n-1)$, *the Trapezoidal Rule (3) is used*

$$I_1^{(k)}(f)=\frac{h}{2}[f(x_k)+f(x_{k+1})],\ k=0,1,\cdots,n-1.$$

The composite Trapezoidal Rule is obtained as

$$T_n=\sum_{k=0}^{n-1}I_1^{(k)}(f)=\sum_{k=0}^{n-1}\frac{h}{2}[f(x_k)+f(x_{k+1})]=\frac{h}{2}[f(a)+2\sum_{k=1}^{n-1}f(x_k)+f(b)].$$

(b) On each subinterval $[x_k,x_{k+1}]$ $(k=0,1,\cdots,n-1)$, *the Simpson's Rule (4) is used*

$$I_2^{(k)}(f)=\frac{h}{6}[f(x_k)+4f(x_{k+\frac{1}{2}})+f(x_{k+1})],\ k=0,1,\cdots,n-1,$$

where $x_{k+\frac{1}{2}}=\frac{x_k+x_{k+1}}{2}$ *is the midpoint of* $[x_k,x_{k+1}]$.

The composite Simpson's Rule is obtained as

$$S_n=\sum_{k=0}^{n-1}I_2^{(k)}(f)=\sum_{k=0}^{n-1}\frac{h}{6}[f(x_k)+4f(x_{k+\frac{1}{2}})+f(x_{k+1})]$$

$$=\frac{h}{6}[f(a)+4\sum_{k=0}^{n-1}f(x_{k+\frac{1}{2}})+2\sum_{k=1}^{n-1}f(x_k)+f(b)].$$

3. Main Results

In numerical integration, interpolation nodes are fixed. For computational efficiency, the integration interval is typically divided into multiple subintervals. The precision of numerical integration depends not only on the order but also on the length of the integration interval. This section presents a method for dividing the integration interval using equal tangent lengths.

Let h be the fixed tangent length, defined as a constant Euclidean length of the tangent line segment at each point along the curve $f(x)$ within the integration interval $[a,b]$. The definition and construction proceed as follows:

Let the integration interval be $[a,b]$, with the initial point $x_0=a$ and $y_0=f(x_0)$. The tangent length at the point (x_0,y_0) is fixed as h, where $h>0$ represents the invariant Euclidean length of the tangent segment at (x_0,y_0). From the endpoint of the tangent segment of length h at (x_0,y_0), draw a perpendicular line to the x-axis. The intersection of this perpendicular with the curve $f(x)$ defines the next point (x_1,y_1), where $y_1=f(x_1)$. At (x_1,y_1), the tangent length remains h. Draw a perpendicular from the endpoint of this tangent segment to the x-axis, and the intersection with $f(x)$ defines (x_2,y_2), where $y_2=f(x_2)$. This iterative process generates a sequence of points (x_k,y_k) $(k=0,1,\cdots,n-1)$ such that the tangent length at each (x_k,y_k) is h, and the perpendicular from the tangent endpoint intersects $f(x)$ at (x_{k+1},y_{k+1}).

Since the slope of $f(x)$ varies across points within $[a,b]$, the projection of h onto the x-axis divides the integration interval $[a,b]$ into several non-equidistant subintervals. Assume the number of non-equidistant subintervals is n, with corresponding nodes defined as:

$$a\le x_0<x_1<x_2<\cdots<x_n\le b,$$

where $f(x)$ takes the function values $y_k = f(x_k)$ $(k = 0,1,\cdots,n-1)$ at these nodes. The inclination angle of $f(x)$ at point (x_k, y_k) is θ_k. The initial point x_0 is selected as the lower bound a of the integration interval $[a,b]$, with no requirement to predefine x_n. The method iteratively computes the non-equidistant nodes x_k based on the tangent length h and the local slope θ_k. The boundary condition is satisfied as x_n approaches the upper bound b through the cumulative effect of the step sizes Δx_{k+1}, ensuring the interval $[a,b]$ is fully covered. This strategy is called equal tangent length, as shown in Figure 1.

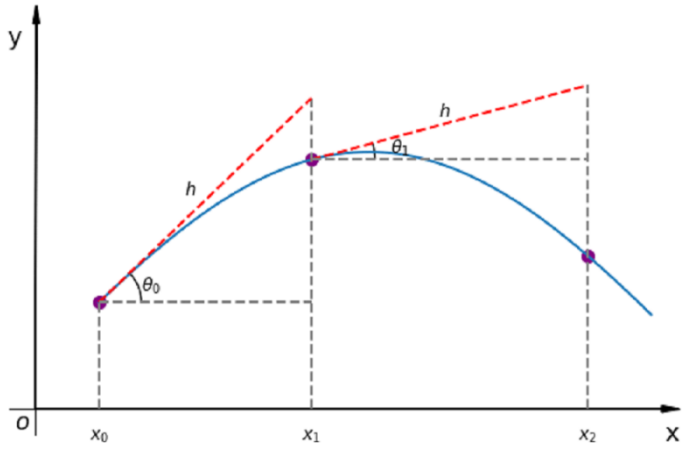

Figure 1. Sketch of the method.

On each subinterval $[x_k, x_{k+1}]$ $(k = 0,1,\cdots,n-1)$, the step size is

$$\Delta x_{k+1} = x_{k+1} - x_k = h\cos\theta_k . \tag{5}$$

Since

$$\tan^2\theta_k = \frac{\sin^2\theta_k}{\cos^2\theta_k} = \frac{1-\cos^2\theta_k}{\cos^2\theta_k} = \frac{1}{\cos^2\theta_k} - 1,$$

we have

$$\cos\theta_k = \frac{1}{\sqrt{1+\tan^2\theta_k}} = \frac{1}{\sqrt{1+[f'(x_k)]^2}}. \tag{6}$$

Substituting formula (6) into formula (5) gives

$$\Delta x_{k+1} = x_{k+1} - x_k = h\cos\theta_k = \frac{h}{\sqrt{1+[f'(x_k)]^2}}, k = 0,1,\cdots,n-1.$$

When $f'(x_k) = 0$, $\cos\theta_k = \dfrac{1}{\sqrt{1+[f'(x_k)]^2}} = 1$, which holds true only for $\theta_k = 0$. For a vertical tangent, $\theta_k = \dfrac{\pi}{2}$ and $\cos\theta_k = 0$, causing $\Delta x_{k+1} = h\cos\theta_k$ in Equation (5) to become zero. An approximation $\Delta y_{k+1} \approx h$ can be used (if $f(x)$ is monotonic at that point), followed by iterative updating via $x_{k+1} = x_k + \dfrac{\Delta y_{k+1}}{[f'(x_{k+1})]}$ (if $f'(x_{k+1}) \neq 0$). The algorithm flowchart is shown in Figure 2.

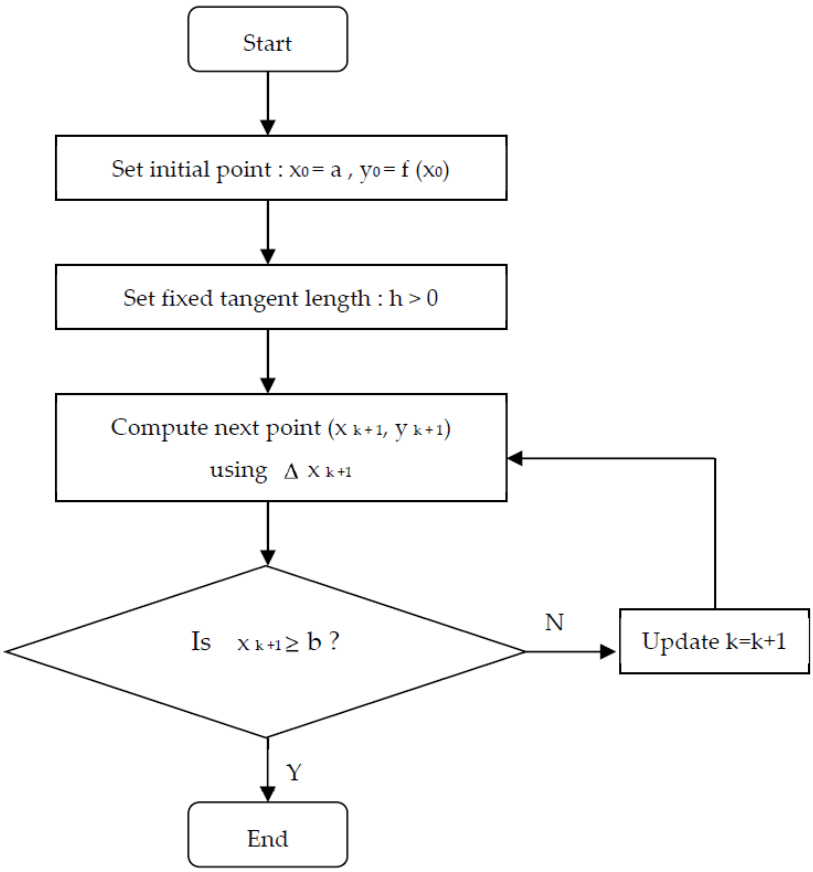

Figure 2. The algorithm flowchart.

3.1. Discussion on the Sensitivity of the Fixed Tangent Length h and Its Impact on Partitioning

When h is excessively large, the tangent length spans a significant portion of the curve, leading to fewer subintervals within $[a,b]$. This reduces the number of nodes (x_k, y_k), as the perpendiculars from the tangent endpoints intersect $f(x)$ at widely spaced points. The step size Δx_{k+1} becomes large where the slope $f'(x_k)$ is small (i.e., $\cos\theta_k \approx 1$), potentially oversimplifying the curve's behavior. In regions of high curvature or rapid change, where $f'(x_k)$ is large, making $\cos\theta_k$ small), Δx_{k+1} may still be substantial, leading to coarse partitioning. This coarseness increases the error in linear approximations, as the method fails to capture local variations, resulting in larger deviations from the exact integral value.

When h is excessively small, the tangent length is minimal, generating a large number of subintervals and densely packed nodes (x_k, y_k). The perpendiculars intersect $f(x)$ at very close points, making Δx_{k+1} small even in regions of varying slope. While this fine partitioning can improve accuracy by better approximating the curve, it significantly increases computational overhead, as seen in the discussion of trade-offs in computational times (e.g., tangent-based partitioning may increase overhead).

The sensitivity of h highlights a trade-off between partitioning resolution and computational cost. An excessively large h leads to coarse partitioning and reduced accuracy, while an excessively small h increases computational overhead with diminishing returns. Practical selection of h should involve an initial estimate based on interval length, adaptive refinement guided by error tolerance, and validation against theoretical error bounds to ensure optimal performance for the given $f(x)$ within $[a,b]$.

Initial Estimation: Start with an initial h based on the interval length and expected function behavior. A reasonable heuristic is $h \approx \frac{b-a}{10}$ to $h \approx \frac{b-a}{50}$, providing a balance between the number of subintervals and computational feasibility, adjustable based on the complexity of $f(x)$.

Adaptive Adjustment: Use an adaptive approach to refine h. Begin with a moderate h and monitor the error (e.g., by comparing with the exact value or a higher-precision method). Reduce h if the error exceeds a

tolerance threshold and increase h if computational time becomes excessive, ensuring a trade-off between accuracy and efficiency.

Validation with Error Bounds: Leverage the theoretical error bounds to validate h. Compute the error for a range of h values and select the smallest h that achieves the desired accuracy without violating computational constraints.

3.2. Numerical Integration Formulas

According to equal tangent length partitioning and Definition 1, we obtain the following numerical integration formulas.

Definition 4 *Assume that the equal tangent length method divides the interval* $[a,b]$ *into* n *parts with step size* $\Delta x_{k+1} = \dfrac{h}{\sqrt{1+[f'(x_k)]^2}}$ *and non-equidistant nodes* $\Delta x_{k+1} = x_{k+1} - x_k$, $k = 0,1,\cdots,n-1$, *then*

(a) On each subinterval $[x_k, x_{k+1}]$ $(k = 0,1,\cdots,n-1)$, *the Trapezoidal Rule (3) is used*

$$\frac{\Delta x_{k+1}}{2}[f(x_k) + f(x_{k+1})], k = 0,1,\cdots,n-1.$$

The new composite Trapezoidal Rule is given by

$$P_n = \sum_{k=0}^{n-1} \frac{\Delta x_{k+1}}{2}[f(x_k) + f(x_{k+1})] = \sum_{k=0}^{n-1} \frac{f(x_k) + f(x_{k+1})}{2} \cdot \frac{h}{\sqrt{1+[f'(x_k)]^2}}. \tag{7}$$

(b) On each subinterval $[x_k, x_{k+1}]$ $(k = 0,1,\cdots,n-1)$, *the Simpson's Rule (4) is used*

$$\frac{\Delta x_{k+1}}{6}[f(x_k) + 4f(x_{k+\frac{1}{2}}) + f(x_{k+1})], k = 0,1,\cdots,n-1,$$

where $x_{k+\frac{1}{2}} = \dfrac{x_k + x_{k+1}}{2}$ *is the midpoint of* $[x_k, x_{k+1}]$. *The new composite Simpson's Rule is given by*

$$\begin{aligned} Q_n &= \sum_{k=0}^{n-1} \frac{\Delta x_{k+1}}{6}[f(x_k) + 4f(x_{k+\frac{1}{2}}) + f(x_{k+1})] \\ &= \sum_{k=0}^{n-1} \frac{1}{6}[f(x_k) + 4f(x_{k+\frac{1}{2}}) + f(x_{k+1})] \cdot \frac{h}{\sqrt{1+[f'(x_k)]^2}}. \end{aligned} \tag{8}$$

It is easy to proof that the two composite numerical integration formulas have recursive relationship. Compact form of the expressions allows its application for numerical problems. We discuss the relationship between P_n and P_{2n}.

$$P_{2n} = \sum_{i=0}^{n-1} \frac{\Delta x_{i+1}}{4}[f(x_i) + 2f(x_{i'}) + f(x_{i+1})] = \frac{1}{2}P_n + \frac{1}{2}\sum_{i=0}^{n-1} \Delta x_{i+1} f(x_{i'}) = \frac{1}{2}(P_n + H_n), \tag{9}$$

where

$$H_n = \sum_{i=0}^{n-1} \Delta x_{i+1} f(x_{i'}) = \sum_{i=0}^{n-1} \Delta x_{i+1} f[a + (2i-1)\frac{b-a}{2n}]. \tag{10}$$

Since $x_{i'} \in (x_i, x_{i+1})$, $\Delta x_{i+1} f(x_{i'})$ is the area of a rectangle with length Δx_{i+1} and height $f(x_{i'})$. $\Delta x_{i+1} f(x_{i'})$ can approximate the integral value of $f(x)$ on $[x_i, x_{i+1}]$. $\Delta x_{i+1} f(x_{i'})$ is the midpoint rule, and H_n is the composite midpoint rule.

Using formula (7) and formula (10) to calculate formula (9) in Definition 4, only the function values at n points need to be computed, reducing the computational burden of the recursive algorithm. Similarly, the recursive algorithm of the new composite Simpson's Rule can reduce the computational burden.

3.3. Remainder Terms

For the purpose of discussion, assume the length of the tangent of $f(x)$ at point (x_0, y_0) is $h = \frac{b-a}{n}$. Since $\Delta x_{k+1} = \frac{h}{\sqrt{1+[f'(x_k)]^2}} \le h \ (k = 0,1,\cdots,n-1)$, the number of subintervals obtained by the method of equal tangent length is not less than n. Assume that h divides the integration interval $[a,b]$ into n^* parts, then $n^* \ge n$.

According to Definition 4, we obtain the remainder terms of composite numerical integration formulas.

Theorem 1 *If $f(x)$ has a second-order continuous derivative on $[a,b]$, the remainder term of the developed composite Trapezoidal Rule meets the condition*

$$\left|I(f) - P_{n^*}\right| \le \frac{n^* M_1}{12} \sum_{k=0}^{n^*-1} (\Delta x_{k+1})^3 \ , k = 0,1,\cdots,n^*-1 .$$

Proof. The remainder term of the new composite Trapezoidal Rule can be obtained from Equation (7)

$$I(f) - P_{n^*} = \sum_{k=0}^{n^*-1} -\frac{f''(\xi_k)}{12} (\Delta x_{k+1})^3 = -\frac{1}{12} \sum_{k=0}^{n^*-1} \frac{f''(\xi_k)}{n^*} \cdot n^* (\Delta x_{k+1})^3 .$$

Since $f''(x)$ is continuous on $[a,b]$, and

$$\min_{0 \le k \le n^*-1} f''(\xi_k) \le \frac{1}{n^*} \sum_{k=0}^{n^*-1} f''(\xi_k) \le \max_{0 \le k \le n^*-1} f''(\xi_k) ,$$

there exists $\xi \in (a,b)$ such that

$$f''(\xi) = \frac{1}{n^*} \sum_{k=0}^{n^*-1} f''(\xi_k) .$$

The remainder term of the new composite Trapezoidal Rule can be expressed as follows

$$I(f) - P_{n^*} = -\frac{n^*}{12} f''(\xi) \sum_{k=0}^{n^*-1} (\Delta x_{k+1})^3 .$$

According to the extreme value theorem, there exists $M_1 > 0$ such that $\left|f''(\xi)\right| \le M_1$, so the remainder term of the new composite Trapezoidal Rule satisfies the inequality

$$\left|I(f) - P_{n^*}\right| \le \frac{n^* M_1}{12} \sum_{k=0}^{n^*-1} (\Delta x_{k+1})^3 \ , k = 0,1,\cdots,n^*-1 .$$

□

Theorem 2 *If $f(x)$ has a fourth-order continuous derivative on $[a,b]$, the remainder term of the new composite Simpson's Rule meets the condition*

$$\left|I(f) - Q_{n^*}\right| \le \frac{n^*}{180} \cdot \frac{M_2}{2^4} \sum_{k=0}^{n^*-1} (\Delta x_{k+1})^5 \ , k = 0,1,\cdots,n^*-1 .$$

Proof. The remainder term of the new composite Simpson's Rule can be obtained from Equation (8)

$$I(f)-Q_{n^*}=\sum_{k=0}^{n^*-1}-\frac{\Delta x_{k+1}}{180}f^{(4)}(\xi_k)(\frac{\Delta x_{k+1}}{2})^4=-\frac{n^*}{180}\sum_{k=0}^{n^*-1}\frac{f^{(4)}(\xi_k)}{n^*}\cdot\frac{(\Delta x_{k+1})^5}{2^4}.$$

Since $f^{(4)}(x)$ is continuous on $[a,b]$, and

$$\min_{0\le k\le n^*-1}f^{(4)}(\xi_k)\le\frac{1}{n^*}\sum_{k=0}^{n^*-1}f^{(4)}(\xi_k)\le\max_{0\le k\le n^*-1}f^{(4)}(\xi_k),$$

there exists $\xi\in(a,b)$, such that

$$f^{(4)}(\xi)=\frac{1}{n^*}\sum_{k=0}^{n^*-1}f^{(4)}(\xi_k).$$

The remainder term of the new composite Simpson's Rule can be expressed as follows

$$I(f)-Q_{n^*}=-\frac{n^*}{180}\cdot\frac{f^{(4)}(\xi)}{2^4}\sum_{k=0}^{n^*-1}(\Delta x_{k+1})^5.$$

According to the extreme value theorem, there exists $M_2>0$ such that $\left|f^{(4)}(\xi)\right|\le M_2$, so the remainder term of the new composite Simpson's Rule satisfies

$$\left|I(f)-Q_{n^*}\right|\le\frac{n^*}{180}\cdot\frac{M_2}{2^4}\sum_{k=0}^{n^*-1}(\Delta x_{k+1})^5,k=0,1,\cdots,n^*-1.$$

□

For the composite numerical integration $I_n(f)$, if there exist $p>0$ and $c\neq0$, the remainder term satisfies

$$\lim_{h\to0}\frac{I(f)-I_n(f)}{h^p}=c.$$

The $I_n(f)$ can converge with degree p.

By the remainder term of Theorem 1 and Theorem 2, when $f''(x)$ and $f^{(4)}(x)$ are continuous on $[a,b]$, the new composite Trapezoidal Rule and new composite Simpson's Rule are convergent, and the convergence orders are 2 and 4 respectively.

In terms of the form of error constants, the new method (equal tangent length) exhibits error constants that depend on the power of subinterval lengths Δx_{k+1} and the dynamic number of subintervals n^*, whereas the error constants of the classical method rely on the fixed interval length $(b-a)$ and a predetermined number of subintervals n. Regarding subinterval partitioning, the new method employs an adaptive step-size strategy, where the subinterval length $\Delta x_{k+1}=\frac{h}{\sqrt{1+[f'(x_k)]^2}}$ is determined by the local derivative $f'(x_k)$, while the classical method adopts a uniform step size $\Delta x=\frac{b-a}{n}$. In terms of error control, the new method automatically reduces the step size in regions with large derivatives (e.g., steep curves), thereby capturing local variations more accurately, whereas the classical method, due to its fixed step size, may introduce larger truncation errors in such regions.

Although the error constants of the new and classical methods share a similar form, the new method achieves higher numerical precision in regions with sharp variations due to its adaptive step-size strategy, whereas the classical method depends on a globally fixed step size. Nevertheless, the new method entails higher computational complexity, as it requires dynamic adjustment of subinterval lengths, which may impact computational efficiency. Therefore, in practical applications, a trade-off between computational accuracy and cost must be considered to select an appropriate numerical integration strategy.

3.4. Discussion on the Behavior of Functions When Continuity Conditions of Derivatives Are Not Satisfied

Theorems 1 and 2 establish the convergence properties of the newly developed composite Trapezoidal Rule and composite Simpson's Rule, respectively. These theorems rely on the assumptions that $f \in \mathrm{C}^2[a,b]$ for the Trapezoidal Rule and $f \in \mathrm{C}^4[a,b]$ for the Simpson's Rule. The error bounds are given by:

(a) For the composite Trapezoidal Rule:

$$\left|I(f)-P_{n^*}\right| \le \frac{n^* M_1}{12}\sum_{k=0}^{n^*-1}(\Delta x_{k+1})^3 \,, k=0,1,\cdots,n^*-1,$$

where M_1 is the bound on $\left|f''(\xi)\right|$.

(b) For the composite Simpson's Rule:

$$\left|I(f)-Q_{n^*}\right| \le \frac{n^*}{180}\cdot\frac{M_2}{2^4}\sum_{k=0}^{n^*-1}(\Delta x_{k+1})^5 \,, k=0,1,\cdots,n^*-1.$$

where M_2 is the bound on $\left|f^{(4)}(\xi)\right|$.

These conditions ensure the convergence orders of 2 and 4, respectively. However, when the second or fourth derivatives are discontinuous, we discusses the resulting behavioral characteristics of $f(x)$ and their implications for the numerical integration methods.

3.4.1. Behavioral Characteristics When $f \notin \mathrm{C}^2[a,b]$

When $f(x)$ does not possess a continuous second derivative on $[a,b]$, the curvature of $f(x)$ exhibits abrupt changes or singularities. This discontinuity may arise from:

(a) Piecewise Functions: For instance, $f(x)=\left|x\right|$ has a discontinuous first derivative at $x=0$, and $f''(x)$ is undefined at that point.

(b) Singularities: Functions like $f(x)=x^{1/3}$ have a second derivative that diverges as $x \to 0$.

In the context of the equal tangent length method, the step size $\Delta x_{k+1}=\dfrac{h}{\sqrt{1+[f'(x_k)]^2}}$ depends on the local slope $f'(x_k)$. Discontinuities in $f''(x)$ can cause $f'(x_k)$ to vary erratically, potentially making the denominator unbounded or zero, thus destabilizing the partitioning of $[a,b]$ into non-equidistant subintervals.

The error bound in Theorem 1 assumes $f''(x)$ is bounded, with $M_1=\max_{x\in[a,b]}\left|f''(x)\right|$. If $f''(x)$ is discontinuous or unbounded, M_1 may not exist, rendering the error estimate invalid. Consequently:

(a) The convergence order of $O(h^2)$ may degrade or be lost entirely.

(b) Near points of discontinuity, the Trapezoidal Rule may overestimate or underestimate the integral, as the linear approximation fails to capture the abrupt curvature changes. For example, integrating $f(x)=\left|x\right|$ over $[-1,1]$ using the Trapezoidal Rule yields significant errors at $x=0$ due to the non-differentiable point.

3.4.2. Behavioral Characteristics When $f \notin \mathrm{C}^4[a,b]$

A lack of continuity in the fourth derivative $f^{(4)}(x)$ indicates that the rate of change of curvature is not smooth, often due to discontinuities in $f'''(x)$ or divergences in $f^{(4)}(x)$. Examples include:

(a) Piecewise Polynomials: A piecewise cubic spline may have a discontinuous $f^{(4)}(x)$ at junction points.

(b) Oscillatory Functions: For $f(x)=x^2\sin(1/x)$ (with $f(0)=0$)), $f^{(4)}(x)$ may become unbounded near $x=0$ due to high-frequency oscillations.

This behavior affects the higher-order accuracy of the Simpson's Rule, which relies on a quadratic approximation over each subinterval.

Theorem 2 requires $f^{(4)}(x)$ to be bounded, with $M_2 = \max_{x\in[a,b]} \left| f^{(4)}(x) \right|$. If $f^{(4)}(x)$ is discontinuous or unbounded:

(a) The expected convergence order of $O(h^4)$ may reduce to $O(h^2)$ or lower, depending on the nature of the discontinuity.

(b) The error bound becomes unreliable, and the method may fail to converge in the presence of severe oscillations or singularities.

When $f \notin \mathrm{C}^2[a,b]$ or $f \notin \mathrm{C}^4[a,b]$, the discontinuities or unboundedness of $f''(x)$ and $f^{(4)}(x)$ lead to degraded performance of the composite Trapezoidal and Simpson's Rules. The methods may lose their guaranteed convergence orders (2 and 4, respectively) and exhibit significant errors near non-smooth points. Employing segment-wise integration or adaptive techniques can mitigate these issues, ensuring more robust numerical integration in the presence of derivative discontinuities.

4. Example

4.1. Experimental Design

To validate the effectiveness of the equal tangent length partitioning method in numerical integration, this study designs a computational example to evaluate its accuracy and convergence by comparing the traditional numerical integration methods with the proposed new composite numerical integration formulas. The integrand chosen for the experiment is $f(x) = e^x$, over the interval [0,1], with the exact integral value given by $\int_0^1 e^x dx = e - 1 \approx 1.718281828459045$. By varying the step size h, the experiment computes the integral approximations of both methods under different partitioning densities and compares them against the exact value to analyze the errors.

In the experiment, the step size h is set to 0.5, 0.25, 0.125, 0.1, 0.0625, 0.05. For each step size, the integral values are calculated using the classical numerical integration methods and the proposed new composite numerical integration formulas, and their absolute errors are recorded. The experimental results are presented through tables and figures to facilitate a clear comparison of the performance of the two methods.

4.2. Experimental Results

4.2.1. Comparison between the Traditional Composite Trapezoidal Rule and the New Composite Trapezoidal Rule

The experimental results are summarized in Table 1, which lists the integral approximations and their corresponding absolute errors for both methods under different step sizes h. The data indicates that as the step size h decreases, the approximations from both methods approach the exact value, but the new composite Trapezoidal Rule consistently demonstrates higher accuracy across all step sizes.

Table 1. Performance of the composite Trapezoidal Rule and the new composite Trapezoidal Rule.

h	The Composite Trapezoidal Rule	Error	The New Composite Trapezoidal Rule	Error
0.5	1.753931092464825	0.035649264005780	1.728626399646955	0.010344571187910
0.25	1.727221904557517	0.008940076098471	1.720694946058797	0.002413117599751
0.125	1.720518592164302	0.002236763705257	1.718864896173384	$5.830677143392471 \times 10^{-4}$
0.1	1.71971349138931	0.00143166293027	1.71845188479423	$1.700563351867412 \times 10^{-4}$
0.0625	1.718841128579994	$5.593001209494020 \times 10^{-4}$	1.718425164421260	$1.433359622153851 \times 10^{-4}$
0.05	1.71863978892522	$3.579604661758662 \times 10^{-4}$	1.71832435054918	$4.252209013011488 \times 10^{-5}$

Figure 3 illustrates the integral values computed by both methods under different h values compared to the exact value. The horizontal axis represents $n = 1/h$, and the vertical axis represents the integral values. It is evident that the approximations from the new composite Trapezoidal Rule (red line) are consistently closer to the exact value (yellow line) than those from the traditional composite Trapezoidal Rule (blue line), with the difference becoming more pronounced at smaller step sizes.

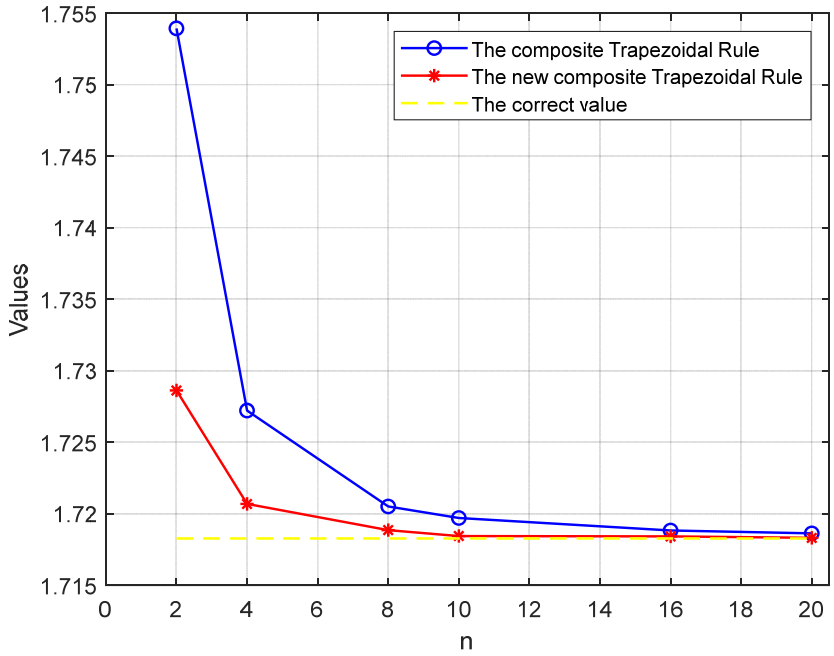

Figure 3. Integral Approximations of the Composite Trapezoidal Rule and the New Composite Trapezoidal Rule Across Different Step Sizes.

Figure 4 further depicts the trend of absolute errors for both methods as $n = 1/h$ increases. The horizontal axis represents n, and the vertical axis represents the absolute error. The y-axis uses a logarithmic scale to better visualize the data. The figure shows that the error of the new composite Trapezoidal Rule (red line) is consistently lower than that of the traditional method (blue line) across all n values. Additionally, while the errors of both methods decrease as n increases, the new method exhibits a faster rate of error reduction.

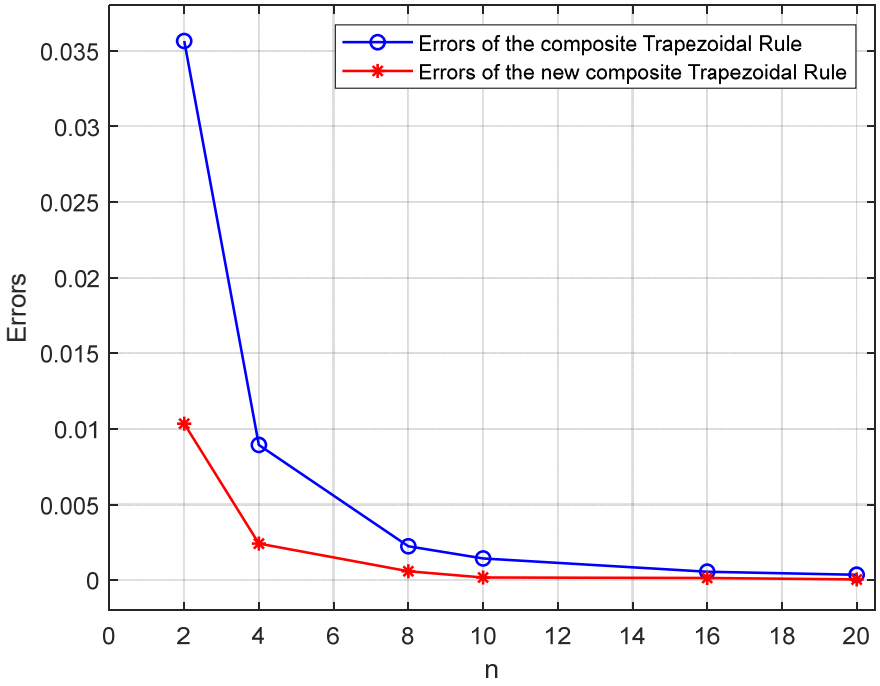

Figure 4. Integral Values of the Composite Trapezoidal Rule and the New Composite Trapezoidal Rule Across Different Step Sizes.

The data from Table 1 and Figure 4 highlight the superior error control of the new composite Trapezoidal Rule. For instance, at $h = 0.125$, the error of the traditional method is 0.022367673057257, whereas the new method's error is only $5.830677143392471 \times 10^{-4}$, representing an error reduction of approximately 97.4%. This advantage persists at smaller step sizes, for example, at $h = 0.05$, the new method's error is about 88.1% lower than that of the traditional method.

From a convergence perspective, the error of the traditional composite Trapezoidal Rule aligns with its theoretical error bound of $O(h^2)$, meaning the error decreases quadratically as the step size h is reduced. This improvement can be attributed to the new method's ability to capture the function's behavior more uniformly across subintervals by balancing the tangent lengths, thereby reducing the error introduced by linear approximations.

4.2.2. Comparison between the Traditional Composite Simpson's Rule and the New Composite Simpson's Rule

The experimental results are presented in Table 2, which details the integral approximations and their corresponding absolute errors for both methods across different step sizes h. The data shows that as h decreases, the approximations from both methods converge toward the exact value, with the new composite Simpson's Rule consistently achieving higher accuracy.

Table 2. Performance of the composite Simpson's Rule and the new composite Simpson's Rule.

h	The Composite Simpson's Rule	Error	The New Composite Simpson's Rule	Error
0.5	1.718318841921747	$3.701346270212902\times10^{-5}$	1.718285777718571	$3.949259526070392\times10^{-6}$
0.25	1.718284154699897	$2.326240851724393\times10^{-6}$	1.718282035513084	$2.070540390253228\times10^{-7}$
0.125	1.718281974051892	$1.455928466675971\times10^{-7}$	1.718281840324412	$1.186536691122342\times10^{-8}$
0.1	1.71828188810386	$5.964481086806472\times10^{-8}$	1.71828182930077	$8.417266883498087\times10^{-10}$
0.0625	1.718281837561772	$9.102726572507436\times10^{-9}$	1.718281829169401	$7.103559962473582\times10^{-10}$
0.05	1.71828183218768	$3.728632291810641\times10^{-9}$	1.71828182851169	$5.263967040036732\times10^{-11}$

Figure 5 illustrates the integral values computed by both methods for varying h, compared to the exact value. The horizontal axis represents $n = 1/h$, and the vertical axis shows the integral values. The new composite Simpson's Rule (pink line) consistently provides approximations closer to the exact value (yellow line) than the traditional composite Simpson's Rule (green line), with the difference becoming more pronounced at smaller step sizes.

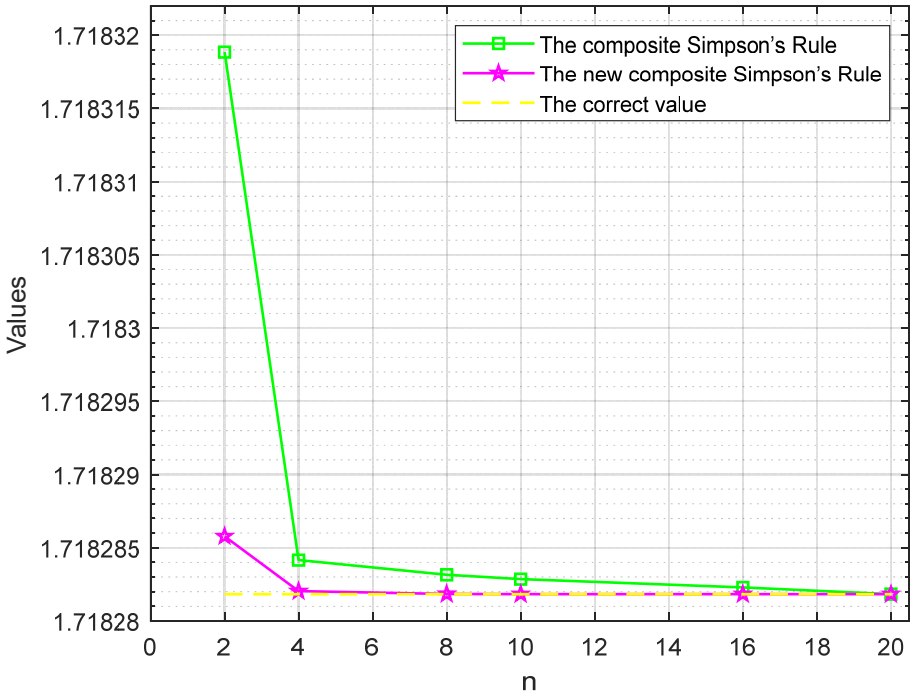

Figure 5. Integral Approximations of the Composite Simpson's Rule and the New Composite Simpson's Rule Across Different Step Sizes.

Figure 6 presents the absolute errors of both methods as $n = 1/h$, using a logarithmic scale for the vertical axis. The horizontal axis represents n, and the vertical axis shows the absolute errors. The y-axis uses a logarithmic scale to better visualize the data.The new composite Simpson's Rule (pink line) exhibits errors that are consistently lower than those of the traditional method (green line) across all n values, with a notably faster rate of error reduction as n increases.

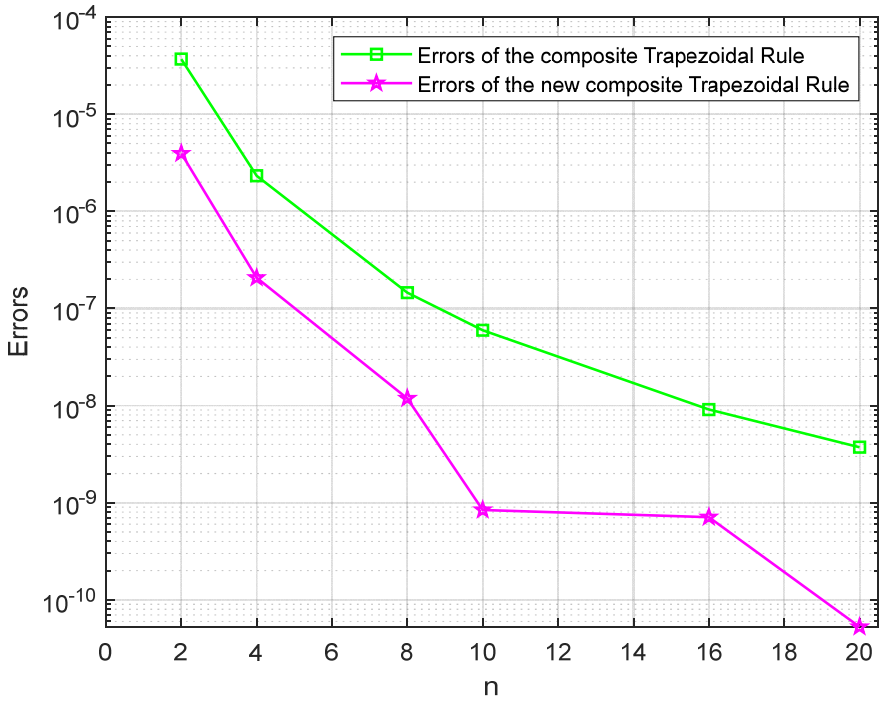

Figure 6. Integral Values of the Composite Simpson's Rule and the New Composite Simpson's Rule Across Different Step Sizes.

The data from Table 2 and Figure 6 highlight the superior error reduction capabilities of the new composite Simpson's Rule. For example, at $h = 0.125$, the error of the traditional method is $1.455928466675071 \times 10^{-7}$, while the new method's error is $1.186536689112324 \times 10^{-8}$, representing an error reduction of approximately 91.9%. At $h = 0.05$, the new method's error is about two orders of magnitude smaller than that of the traditional method, with an error of $5.263967040036732 \times 10^{-11}$, compared to $3.728632918610641 \times 10^{-9}$.

From a convergence perspective, the traditional composite Simpson's Rule follows its theoretical error bound of $O(h^4)$, indicating a quartic error reduction as the step size h decreases. The new composite Simpson's Rule, however, demonstrates an even faster convergence rate, as evidenced by the steeper slope of the error curve in Figure 5. This suggests that the equal tangent length partitioning method achieves a higher-order error term, likely due to its ability to distribute subintervals more effectively based on the function's geometric properties, thereby reducing the truncation error.

4.3. Experimental Discussion

The experimental results confirm the efficacy of the equal tangent length partitioning method in improving the accuracy of numerical integration. The new composite numerical integration outperforms the traditional method across all tested step sizes, with significant error reductions, particularly at larger step sizes (e.g., $h = 0.5$). This indicates that the new method maintains high accuracy even with fewer subintervals, showcasing its robustness.

Additionally, this experiment focuses on the smooth function e^x, and the performance of the new method on less smooth or highly oscillatory functions remains to be explored. Future research could investigate adaptive partitioning strategies to further enhance the method's applicability across diverse integrands.

5. Results and Discussion

The experimental results presented in Tables 1 and 2, along with Figures 3–6, clearly demonstrate the effectiveness of the equal tangent length partitioning method. Both new composite formulas consistently outperform their classical counterparts across all tested step sizes. Notably, the new composite Trapezoidal Rule achieved a maximum error reduction of approximately 97.4% compared to the classical composite Trapezoidal Rule (at $h = 0.125$), while the new composite Simpson's Rule achieved an error reduction of about 91.9% (at $h = 0.5$). This performance gain is especially significant at coarser partitions, indicating that the proposed

method provides higher accuracy even with fewer subintervals. The key to this improvement lies in the adaptive nature of the partitioning strategy, which dynamically adjusts subinterval lengths based on the local derivative $\left|f'(x_k)\right|$. In regions where the function is relatively flat (small $\left|f'\right|$), the step size Δx_{k+1} increases, reducing unnecessary computational points. Conversely, in regions of high curvature or steep slopes (large $\left|f'\right|$), the step size decreases, allowing the method to capture finer details of the function's behavior. This intrinsic adaptability leads to a more balanced error distribution across the integration interval, unlike the classical methods which employ a uniform step size and can suffer from larger local truncation errors in rapidly varying regions.

Furthermore, the convergence analysis confirms the theoretical error bounds established in Theorems 1 and 2. The error plots (Figures 4 and 6) show steeper slopes for the new methods on a logarithmic scale, visually confirming their superior convergence rates. While the classical composite Trapezoidal and Simpson's Rules converge with orders $O(h^2)$ and $O(h^4)$ respectively, the new methods exhibit error constants that depend dynamically on the subinterval lengths and the number of partitions m. This results in an effective higher-order convergence behavior in practice, as evidenced by the significantly smaller absolute errors at comparable step sizes. It is important to note, however, that this increased accuracy comes with a trade-off: the need to compute the derivative $f'(x_k)$ at each partition point and the iterative process to determine Δx_{k+1} introduce additional computational overhead compared to the straightforward classical methods. Therefore, the choice between the new and classical methods should be guided by the specific requirements of the problem—prioritizing accuracy in contexts where function evaluations are inexpensive but high precision is critical, or favoring speed in large-scale computations where moderate error is acceptable.

6. Conclusions

This study has introduced a novel partitioning strategy for numerical integration based on the principle of equal tangent lengths. The primary contributions of this work are threefold. First, we have developed a new geometric approach to interval partitioning that moves beyond traditional equidistant nodes. By maintaining a constant Euclidean tangent length h along the curve, the method generates a set of non-equidistant nodes $\{x_k\}$ where the step size Δx_{k+1} is adaptively determined by the local slope $f'(x_k)$. This is visually summarized in the conceptual sketch (Figure 1) and the algorithmic flowchart (Figure 2). Second, leveraging this adaptive partitioning, we have derived two new composite numerical integration formulas: a composite Trapezoidal Rule (Equation (7)) and a composite Simpson's Rule (Equation (8)). Third, we have provided a rigorous theoretical foundation for these formulas, establishing their error bounds (Theorems 1 and 2) and proving their convergence with orders 2 and 4, respectively, under standard smoothness assumptions.

The experimental validation, comprehensively detailed through Tables 1 and 2 and Figures 3–6, underscores the practical significance of our contributions. A direct comparison with classical methods reveals the superior performance of the proposed approach. For the integrand $f(x)=e^{x^2}$ on [0,1], the new composite Trapezoidal Rule reduced the absolute error by up to 97.4% compared to the classical composite Trapezoidal Rule, while the new composite Simpson's Rule achieved error reductions up to 91.9%. The graphical evidence in Figures 3 and 5 shows that approximations from the new methods consistently lie closer to the exact integral value across all step sizes. Furthermore, the error trends plotted in Figures 4 and 6 (log scale) demonstrate not only lower error magnitudes but also steeper convergence slopes for the new methods, confirming their enhanced efficiency in error reduction.

In conclusion, the equal tangent length partitioning method presents a significant and effective advancement in numerical integration. It successfully addresses a key limitation of classical methods—their inflexible, uniform partitioning—by introducing an adaptive, geometry-informed strategy. While the method exhibits increased computational complexity due to derivative evaluations and iterative node placement, the substantial gains in accuracy, particularly for functions with varying curvature, make it a valuable tool for applications demanding high-precision integration. Future work could explore optimizing the selection of the tangent length h, extending the method to higher-order formulas or multidimensional integrals, and testing its robustness on functions with discontinuities or singularities.

Author Contributions

J.S.: Conceptualization, Methodology, Software, Formal analysis, Investigation, Writing—original draft, Writing—review & editing, Visualization. W.S.: Software, Validation, Formal analysis, Investigation, Data curation, Writing—review & editing, Visualization. M.S.: Methodology, Formal analysis, Investigation,

Writing—original draft, Writing—review & editing, Supervision. All authors have read and approved the final version of the manuscript.

Funding

This research was supported by the Science and Technology Plan Fund Project of the Fujian Provincial Department of Science and Technology, China (No. 2024H0038), the Scientific Research and Innovation Team of Minnan University of Science and Technology (No. 2024XTD160) and the Key Laboratory of IoT Intelligent Control for Universities of Fujian Province.

Institutional Review Board Statement

Not applicable.

Informed Consent Statement

Not applicable.

Data Availability Statement

No new data were created or analyzed in this study. Data sharing is not applicable to this article.

Conflicts of Interest

No conflict of interest exists in the submission of this manuscript, and the manuscript is approved by all authors for publication. I would like to declare on behalf of my co-authors that the work described was original research that has not been published previously, and not under consideration for publication elsewhere, in whole or in part. All the authors listed have approved the manuscript that is enclosed. We declare that we have no financial and personal relationships with other people or organizations that can inappropriately influence our work, there is no professional or other personal interest of any nature or kind in any product, service and/or company that could be construed as influencing the position presented in, or the review of, the manuscript entitled.

Use of AI and AI-Assisted Technologies

No AI tools were utilized for this paper.

References

1. Mamatha, M.; Venkatesh, B.; Kumar, P.S.; et al. Numerical integration of some arbitrary functions over an ellipsoid using Gaussian quadrature rules. *Int. J. Chem. Eng.* **2024**, *2024*, 5321249.
2. Zecevic, M.; Lebensohn, R.A. Approximation of periodic green's operator in real space using numerical integration and its use in fast fourier transform-based micromechanical models. *Int. J. Numer. Methods Eng.* **2021**, *122*, 7536–7552.
3. Jakub Prüher; Karvonen, T.; Oates, C.J.; et al. Improved calibration of numerical integration error in sigma-point filters. *IEEE Trans. Autom. Control* **2021**, *66*, 1286–1292.
4. Banica, V.; Maierhofer, G.; Schratz, K. Numerical integration of schrdinger maps via the hasimoto transform. *SIAM J. Numer. Anal.* **2024**, *62*, 322–352.
5. Yáñez, D.F. Numerical integration rules based on B-spline bases. *Appl. Math. Lett.* **2024**, *156*, 109142.
6. Xia, Y.; Wan, Y.; Su, G.; et al. An improved numerical integration method for prediction of milling stability using the lagrange-simpson interpolation scheme. *Int. J. Adv. Manuf. Technol.* **2022**, *120*, 8105–8115.
7. Moheuddin, M.M.; Uddin, M.J.; Kowsher, M. A new study to find out the best computational method for solving the nonlinear equation. *Appl. Math. Sci. Int. J.* **2019**, *6*, 15–31.
8. Maure, O.P.; Mungkasi, S. Application of numerical integration in solving a reverse osmosis model. *AIP Conf. Proc.* **2019**, *2202*, 020043.
9. Altwallbah, N.M.M.; Radzi, M.A.M.; Azis, N.; et al. New perturb and observe algorithm based on trapezoidal rule: Uniform and partial shading conditions. *Energy Convers. Manag.* **2022**, *264*, 115738.
10. Georgiev, S.G.; Erhan, N.M. The taylor series method and trapezoidal rule on time scales. *Appl. Math. Comput.* **2020**, *378*, 125200.
11. Zhu, C.; Li, C. *Numerical Approximation and Computational Geometry*, 1st ed.; Higher Education Press: Beijing, China, 2020; pp. 171–206.